



HAL
open science

A complete characterization of the structure of the vesicular phase in AOT - Brine system in the diluted region of the phase diagram

Julie Wolanin, Loïc Barré, Christine Dalmazzone, Daniela Bauer

► **To cite this version:**

Julie Wolanin, Loïc Barré, Christine Dalmazzone, Daniela Bauer. A complete characterization of the structure of the vesicular phase in AOT - Brine system in the diluted region of the phase diagram. *Colloids and Surfaces A: Physicochemical and Engineering Aspects*, 2018, 559, pp.218 - 225. 10.1016/j.colsurfa.2018.09.052 . hal-01931316

HAL Id: hal-01931316

<https://ifp.hal.science/hal-01931316>

Submitted on 30 Nov 2018

HAL is a multi-disciplinary open access archive for the deposit and dissemination of scientific research documents, whether they are published or not. The documents may come from teaching and research institutions in France or abroad, or from public or private research centers.

L'archive ouverte pluridisciplinaire **HAL**, est destinée au dépôt et à la diffusion de documents scientifiques de niveau recherche, publiés ou non, émanant des établissements d'enseignement et de recherche français ou étrangers, des laboratoires publics ou privés.

Title.

A complete characterization of the structure of the vesicular phase in AOT – Brine System in the diluted region of the phase diagram.

Author names and affiliations.

Julie WOLANIN^a, Loïc BARRE^a, Christine DALMAZZONE^a, Daniela BAUER^a

^a IFP Energies nouvelles, 1 et 4 avenue du Bois-Préau, 92852, Rueil Malmaison, France

Corresponding author. Christine DALMAZZONE (email: christine.dalmazzone@ifp.fr ; postal address: IFP Energies nouvelles, 1 et 4 avenue du Bois-Préau, 92852, Rueil Malmaison, France)

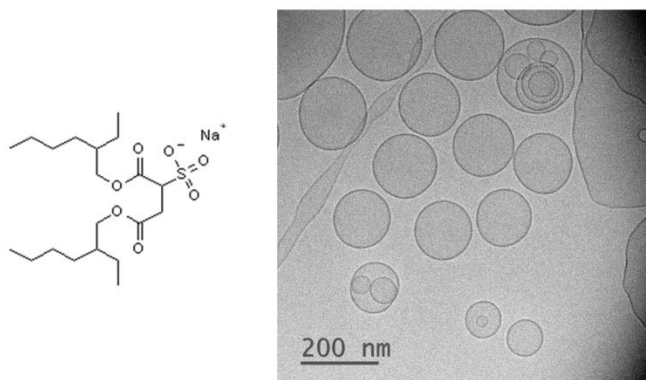
Keywords.

Surfactant; AOT vesicle; bilayer; phase diagram; scattering techniques; cryo-TEM.

Abstract.

The structure of vesicles formed by anionic surfactant sodium bis(2-ethylhexyl) sulfosuccinate (AOT) in brine solution (1.5 wt% NaCl) at 20°C, in the diluted region of the phase diagram, has been characterized by cryogenic transmission electron microscopy (cryo-TEM) and the combination of three scattering techniques (Small Angle X-ray Scattering (SAXS), Dynamic Light Scattering (DLS) and Multi-angle light scattering (MALS)). Results show a polydisperse vesicle size system. The distribution is mainly composed of small vesicles (14 nm diameter) and there is no micelles in solution. The determination of the form factor indicates the presence of only spherical vesicles (no other morphologies, such as tubular vesicles, were observed). The bilayer structure of the vesicles was characterized by SAXS and the membrane thickness measured at 2.7 nm. This thickness is shorter than twice the AOT molecule extended length indicating a non-negligible interpenetration of the hydrophobic tails.

Graphical abstract.



1. Introduction

Due to its very useful physicochemical properties like nontoxicity, significant impact on the interfacial tension or its capacity to form normal and reverse micelles in solution, the anionic surfactant AOT (sodium bis(2-ethyl-1-hexyl)sulfosuccinate) is used in a wide range of applications in chemistry and biochemistry. Common examples are formulations, lubrication, solubilization, emulsification and cleaning. Also AOT has been widely studied in brine because of its ability to form microemulsions with oil and water. Indeed, there is no need of additional co-surfactant as it would be the case for the majority of surfactants. Microemulsification processes are used in a large number of applications such as oil recovery or detergency. Thus, it is necessary to understand the equilibrium phase behavior of surfactant/brine systems as they induce ultralow oil-water interfacial tensions required for the formation of microemulsions. AOT can form microemulsions at low surfactant concentration.

However, the addition of salt can significantly impact the characteristics of AOT microemulsions. Thus, a thorough understanding of the surfactant aggregation behavior in brine is essential.

Due to its geometry (small hydrophilic head group and bulky hydrophobic group), AOT is not well solubilized in water and the phase diagram for the AOT/water/NaCl system is dominated by the coexistence of the lamellar phase (L_α) and the sponge phase (L_3). The AOT/water/NaCl system for a low concentration of salt in the water-rich region has already been investigated for many years [1–7]. Gosh et al.[2] have studied the AOT phase diagram in the diluted domain (Figure 1) analyzing 80 solutions of different compositions with polarizing microscopy.

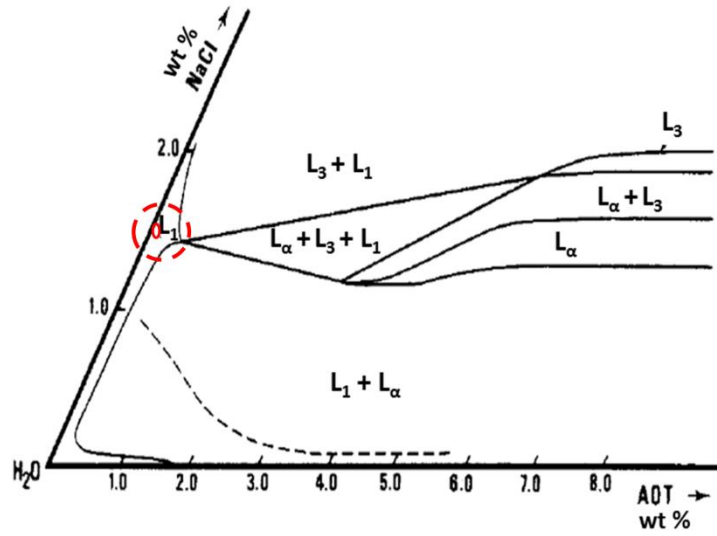


Figure 1: AOT-NaCl-H₂O phase diagram at 30 °C according to ref[2] at low salinity - L₁: isotropic solution; L_α: lamellar phase and L₃: sponge phase; (---) unstable and stable (below and above the dashed line respectively) dispersions of spherulites; (◦) is the composition investigated; (---) diluted region investigated in the current work (Adapted with permission from J. Phys. Chem. 91 (17) (1987) 4528–4535. Copyright (2018) American Chemical Society)

According to the phase diagram, the existence of the optically isotropic phase L₁, known as the micellar phase, is restricted to an AOT concentration of ≈ 1.8wt% with no electrolyte addition at 30°C. The structure of aggregates (such as micelles or vesicles) formed in L₁ has not been considered by Gosh et al. since they were only interested in the effect of salt addition on the phase behavior and defining phase boundaries. A two-phase region (L₁ + L_α) appears at low surfactant concentration above 1.8wt%. The single lamellar phase L_α prevails in the phase diagram at higher surfactant concentrations (>20wt%) [4,8]. In this work, we considered a composition in the ultra-diluted region of the phase diagram (red circle in Figure 1).

The geometry of surfactant aggregates can be predicted by the calculation of the molecular packing parameter:

$$p = \frac{V_H}{a_0 l_c} \quad (1)$$

This parameter depends on both the length l_c and molecular volume V_H of the hydrophobic group; and on the optimal cross-sectional area of the hydrophilic head a_0 of the surfactant molecule. Vesicles are formed when the packing parameter is comprised between 0.5 and 1. The AOT hydrophobic group is composed of two tails creating a voluminous hydrophobic

group V_H which allows the formation of vesicles in solution ($p \approx 0.65$). The addition of salt tends to decrease the hydrophilic area a_0 , favoring the spontaneous formation of vesicles.

In the literature, different shapes and dimensions of AOT aggregates in aqueous or brine solutions have been reported: micelles [9–12], vesicles [7,9,13–19], lamellar phase[2–6,20–22], and sponge phase[1,23]. Double-tailed surfactants are commonly supposed to form lamellar liquid crystals in water: most of them form an isotropic micellar phase at very low surfactant concentration before attaining the lamellar phase[24]. For poorly soluble surfactants as AOT, the following transitions are generally observed: from vesicles (at high dilution) to lamellar dispersion (ex: spherulites for AOT surfactant[2]) and finally to single lamellar phase[17]. Regev et al.[17] have demonstrated the following transition for AOT in water: unilamellar vesicles \rightarrow double-lamellar vesicles \rightarrow long double-wall tubules \rightarrow lamellar liquid crystal.

The diluted region in the micellar phase L_1 (optically isotropic fluid) of the phase diagram has been insufficiently characterized and complementary studies seem to be necessary. At very low surfactant concentration, near the Critical Micelle Concentration (CMC), the existence of vesicles (energetically favorable) rather than micelles has been reported for the AOT/water/NaCl system[15–17,25,26]. Vesicles have been revealed by microscopy techniques such as cryogenic transmission electron microscopy and optical microscopy. Sheu et al.[10] have demonstrated by small angle neutron scattering measurements that micelles form between 0.2wt% and 1wt% with a micelle morphology transiting from spherical to oblate spheroidal. The pure micellar phase is clearly restricted and an equilibrium appears quickly between micelles and vesicles increasing the surfactant concentration to in fine form a single vesicular phase. The Critical Vesicle Concentration (CVC) has been measured by microcalorimetry, electrical conductivity and fluorescence at 7.5 mM (0.3wt%) corresponding to the transition of AOT micelles to vesicles[9,26] with no salt addition.

Cryo-TEM and phase-contrast microscopy experiments have shown that the dilute region (ultra-low surfactant and salt concentrations) contains highly polydispersed vesicles in terms of size and number of bilayers[15–17]. Shahidzadeh et al.[16] have shown that the vesicular structure is clearly affected by the salt concentration: spherulites are observed at low salinity (<0.2wt% NaCl) while tubular vesicles form at higher salinity (> 0.4wt% NaCl). Grillo et al.[13] have demonstrated that the vesicle radius decreases (from 40 nm to 28 nm) with increasing sodium chloride concentration (from 0.12wt% to 1wt% respectively). Shahidzadeh et al.[16] have studied various compositions at ultra-low surfactant concentrations demonstrating the presence of vesicles in brine solution using phase-contrast microscopy.

Vesicle size characterization is limited with this technique and small aggregates (< 100 nm) cannot be well investigated.

In this paper, we proposed a complete characterization of the vesicular system such as the surfactant morphology as well as their size distribution at ultra-low surfactant concentration. The combination of the three scattering methods (SAXS, DLS and MALS) provides a characterization of surfactant aggregates structure at different length scales.

This preliminary study of the AOT vesicular system is necessary because further measurements are being performed in attempt to understand the adsorption of AOT vesicles formed in brine on silica. Although silica is negatively charged in neutral conditions, we witnessed the adsorption of AOT vesicles on silica during our experimentations. Surfactant adsorption phenomena in an electrostatic repulsive environment can happen in many industrial applications such as enhanced oil recovery processes, in which silica is frequently used to mimic reservoir rocks.

2. Materials and Methods

2.1. Materials

Aerosol-OT, usually called AOT (sodium bis(2-ethyl-1-hexyl)sulfosuccinate, $C_{20}H_{37}NaO_7S$) was purchased from Sigma-Aldrich (BioXtra, $\geq 99\%$, product number D4422, batch no. SLBL8632V) and used as received. The chemical structure of AOT is shown in Figure 2. AOT is composed of a negatively charged hydrophilic head group ($C_4H_7NaO_7S$) and of a hydrophobic group consisting of two tails (C_8H_{15}). Aqueous surfactant solutions were prepared in Milli-Q® water named mQ water (ultrapure water.).

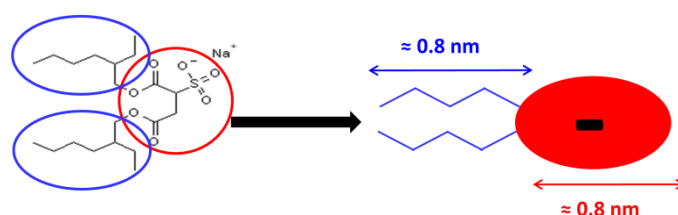


Figure 2: Chemical structure of AOT

2.2. Methods

2.2.1. Determination of the Critical Micelle Concentration (CMC)

The critical micelle concentration (CMC) of AOT in mQ water and the critical vesicle concentration (CVC) in brine 1.5wt% NaCl was measured using the Wilhelmy plate

technique. The surface tension of surfactant solutions (≈ 20 mL) was measured at 20°C by a Wilhelmy plate tensiometer (Force tensiometer K100© Krüss) with a platinum plate (Krüss Standard Plate, PL 01). The CMC and CVC were measured two times and the average values were reported.

2.2.2. Cryo-Transmission Electron Microscopy (Cryo-TEM)

Cryo-TEM measurements were performed at Solvay Research & Innovation Centre (Aubervilliers, France). Sample preparation for cryo-TEM implicated a vitrification procedure. A drop of the surfactant solution were spread on a copper grid covered by a Lacey Formvar carbon film 200 mesh (Ted Pella). Excess liquid was blotted with a filter paper on a Vitrobot™ (FEI) to obtain a thin liquid film on the grid. The sample was then plunged in liquid ethane cooled by liquid nitrogen. The vitrified sample was then transferred into the vacuum column of the TEM microscope (TEM JEM 1400 operating at 120 kV) under nitrogen atmosphere.

2.2.3. Scattering techniques

The principle of scattering techniques consists in the acquisition of the scattered intensity as a function of the scattering vector Q given by:

$$Q = \frac{4\pi n \sin \theta}{\lambda_0} \quad (2)$$

with λ_0 the wavelength of the incident beam in vacuum, n the refractive index ($n=1$ in SAXS and $n=1.33$ in light scattering) and 2θ the scattering angle. In order to investigate the membrane and vesicle structure, we combine SAXS and MALS measurements to collect the scattering intensities over a wide range of Q -values. The determination of the overall size is possible at low Q -range. At intermediate Q range, the vesicular shape is identified and the characterization of the bilayer structure is obtained at high Q range. DLS gives the vesicle size distribution.

2.2.3.1. Multi-angle Light Scattering (MALS)

Measurements were performed on a spectro-goniometer SEM-CLASSICAL. The instrument is equipped with a diode laser operating at an output power of 3.5 mW. The incident beam ($\lambda_0=658$ nm) is polarized vertically with reference to the scattering plane. The scattering intensity of the surfactant solution $I_{M,2}(Q)$ is measured as a function of the scattering vector Q : the scattering angle is varied from 20° to 140° corresponding to a Q -range from $3.3 \times 10^{-3} \text{ nm}^{-1}$ to $1.8 \times 10^{-2} \text{ nm}^{-1}$. The Rayleigh ratio $R(Q)$ is calculated using toluene as reference as follows:

$$R(Q) = \frac{I_{M,2}(Q) - I_{M,1}(Q)}{I_{M,toluene}} R_{toluène} \left(\frac{n_1}{n_{toluene}} \right)^2 \quad (3)$$

with $I_{M,1}(Q)$ the scattering intensity of brine solution and $I_{M,toluene}$ the scattering intensity of toluene at $2\theta=90^\circ$, n_1 and $n_{toluene}$ the refractive index of the solvent (1.33) and toluene (1.49) respectively at 20°C .

The Rayleigh ratio is given by:

$$R(Q) = KCM_W P_{Light}(Q)S(Q) \quad (4)$$

with $P_{Light}(Q)$ the form factor, $S(Q)$ the structure factor, M_W the weight-average molecular weight and C the surfactant concentration. In the case of dilute solutions with no inter-particle interactions $S(Q) \approx 1$.

K is defined as:

$$K = \frac{2\pi^2 n_1^2 \left(\frac{\partial n}{\partial c} \right)^2}{\lambda_0^4 N_A} \quad (5)$$

with N_A the Avogadro's number and $\left(\frac{\partial n}{\partial c} \right)$ the refractive number increment. $\left(\frac{\partial n}{\partial c} \right)$ for AOT solutions were measured with an Anton Paar refractometer operating at room temperature: a value of $0.124 \text{ cm}^3 \cdot \text{g}^{-1}$ has been obtained.

A more detailed description of the technique can be found in the literature[27].

2.2.3.2. Small angle X-ray scattering (SAXS)

Small-angle X ray scattering measurements were carried out at the SWING beamline of Synchrotron SOLEIL (Gif-sur-Yvette, France). Data were collected at two different configurations (Table 1) chosen to cover the $0.3 - 10.7 \text{ nm}^{-1}$ Q range at 20°C .

Table 1: SAXS configurations chosen

	Conf 1	Conf 2
Incident beam λ [Å]	0.78	1.24
Sample-to-detector distance [m]	0.55	6

The calibration was performed with silver behenate. The absolute intensities were obtained by normalization with respect to brine solution.

Absolute scattered intensity $I_X(Q)$ of a monodisperse sample is given by:

$$I_X(Q) = \phi V \Delta \rho^2 P_X(Q) \quad (6)$$

with ϕ the volume fraction of aggregates dispersed in solution, V their volume, $\Delta\rho$ the scattering length density difference between the solvent and surfactant aggregates and $P_X(Q)$ the form factor of surfactant aggregates.

In the case of a polydisperse sample, the global scattering intensity $I_X(Q)$ is defined as:

$$I_X(Q) = \phi \Delta\rho^2 V \int_0^{\infty} P(Q, R) f(R) dR \quad (7)$$

with $f(R)$ being the size distribution function.

The electronic scattering length density is calculated as follows:

$$\rho_e = \frac{r_e}{V_m} \sum_i n_i Z_i \quad (8)$$

with $r_e = 2.81 \times 10^{-13}$ cm the classical radius of the electron, V_m the molecular volume, Z_i is the atomic number of the i th atom and n_i the number of the i th atom. Results are given in Table 2.

Table 2: X-ray Scattering Length Density of materials used

Materials	Formula	$\rho_e \times 10^{10}$ [cm ⁻²]
Solvent	H ₂ O	9.42
AOT head group	C ₄ H ₃ NaO ₇ S	16.2
AOT tails	(C ₈ H ₁₇) ₂	7.63

A more detailed description of the technique can be found in the literature [28].

2.2.3.3. Dynamic Light Scattering (DLS)

The size of surfactant aggregate was studied with a DLS setup of Cordouan technologies. The surfactant solution was set in a quartz cell illuminated by a laser beam ($\lambda_0 = 658$ nm). The fluctuations of the scattered light intensity with time were collected by a photodetector (avalanche photodiode) at a fixed scattering angle (90°). The optical signal collected corresponds to temporal intensity fluctuations of the scattered light, caused by the random Brownian motion of aggregates. The autocorrelation function of the scattered intensity $G_2(Q, \tau)$ is measured as a function of Q .

The Siegert relation equates $G_2(Q, \tau)$ with the normalized electric field autocorrelation function $g_1(Q, t)$ which describes correlated particle motions:

$$G_2(Q, \tau) = \alpha + \beta g_1^2(Q, \tau) \quad (9)$$

where α is the baseline and β the coherence factor. In the case of a polydisperse system, $g_1(Q, \tau)$ can be expressed as a sum of exponentially decaying functions:

$$g_1(Q, \tau) = \sum_i A_i e^{-D_i Q^2 \tau} \quad (10)$$

where A_i is the scattered intensity contribution of particles i and D_i its diffusion coefficients. All D_i were calculated by fitting the autocorrelation function $G_2(Q, \tau)$ using inversion Pade-Laplace algorithm.

Finally, considering isolated Brownian spheres well dispersed in solution, the hydrodynamic radius R_{h_i} of a sphere can be calculated from the diffusion coefficient using the Stokes-Einstein equation:

$$D_i = \frac{k_B T}{6\pi\eta R_{h_i}} \quad (11)$$

where k_B is the Boltzmann constant, η the solvent dynamic viscosity and T the temperature. A more detailed description of the technique can be found in the literature[29].

3. Theory : Expression of vesicle form factor for light $P_{Light}(Q)$ and X-ray $P_X(Q)$ scattering

3.1. Light scattering

In the literature[30–36], unilamellar vesicles are assimilated to isotropic hollow spheres and analyzed within the Rayleigh-Gans-Debye (RGD) approximation. This approximation is based on two assumptions:

- the difference in refraction index between the solvent and the vesicle membrane is very small : variations in the local electric field are negligible when light passes through the vesicle membrane
- the size of vesicles is smaller than the wavelength of light : the incident electric field is the same in all parts of the scattering vesicle volume

These two conditions are summarized as:

$$L \ll \frac{\lambda}{|1 - n_2/n_1|} \quad (12)$$

with L being the particle size, n_1 and n_2 the refractive index of the solvent and vesicle membrane respectively.

Hallet et al.[31] have compared the relative scattering intensities for a vesicle system calculated with RGD approximation and Mie theory. They have demonstrated that RGD

approximation is adequate and sufficient to interpret vesicle scattering in the range of validity of equation (12).

The form factor $P_{Light}(Q)$ for spherical vesicles (hollow spheres) in the RGD approximation can be written:

$$P_{Light}(Q) = \left(\frac{3}{Q^3(R_o^3 - R_i^3)} (\sin QR_o - \sin QR_i - QR_o \cos QR_o + QR_i \cos QR_i) \right)^2 \quad (13)$$

with R_o and R_i the outer and inner radius respectively, of the vesicle.

For unilamellar vesicle smaller than the micron with an infinitely thin membrane (< 10 nm), the form factor can be reduced to:

$$P(Q) = \left(\frac{\sin(QR_o)}{QR_o} \right)^2 \quad (14)$$

3.2. X-ray scattering

For SAXS measurements, the form factor $P_X(Q)$ for vesicles is the same as in equation (13). In the measured Q-range (high Q domain), the bilayer structure is explored. We can separate the electronic scattering length density profiles of the head groups from the hydrophobic part in the expression of the form factor. The final form of the scattering intensity can be written:

$$\begin{aligned} I_X(Q) = & (B(Q, R_o, \rho_{sol} - \rho_h) + B(Q, R_o + d_h, \rho_h - \rho_t) \\ & + B(Q, R_o + d_h + d_t, \rho_t - \rho_h) + B(Q, R_o + 2d_h \\ & + d_t, \rho_h - \rho_{sol}))^2 \end{aligned} \quad (15)$$

with d_h and d_t thicknesses of hydrophilic and hydrophobic parts respectively of the bilayer, ρ_{sol} , ρ_h and ρ_t the scattering length density of the solvent, hydrophilic and hydrophobic parts and $B(Q, R, \Delta\rho)$:

$$B(Q, R, \Delta\rho) = \frac{4}{3} \pi R^3 \Delta\rho \frac{\sin QR - QR \cos QR}{(QR)^3} \quad (16)$$

4. Results and Discussion

4.1. CMC Determination

CMC of AOT in mQ water and the CVC in brine 1.5wt% NaCl are shown in Table 3. CMC values in mQ water found in the literature (0.11wt%[37] and 0.14wt%[38]) are in good agreement with our experimental data. Small differences observed might be explained by the presence of some impurities in AOT. As expected, the addition of NaCl lowers the CVC

because of the screening of the surfactant charges (decrease of electrostatic repulsion between sulfonate head groups).

Table 3. Critical Micelle Concentration measured at 20°C

	Experimental data
AOT in mQ water [wt%]	0.1 ± 0.01
AOT in brine 1.5wt% NaCl [wt%]	0.009 ± 0.001

4.2. Cryo-TEM

We performed CryoTEM measurements to identify the morphology of AOT aggregates formed in brine solution. In order to enhance the visibility of surfactant aggregates, we investigated a very concentrated AOT solution at 55CVC (0.5wt%). Figure 3 illustrates a large number of spherical unilamellar vesicles of different sizes. We can observe a small fraction of non-spherical vesicles in Figure 3 such as tubular vesicles. Vesicles membranes being highly flexible, vesicle deformation and membrane invagination can occur during the vitrification process. Kuntsche et al. [39] have assumed that the osmotic imbalance between the inner and outer aqueous phase of the vesicle taking place during the freezing process is the principal origin of vesicles deformation and rearrangement.

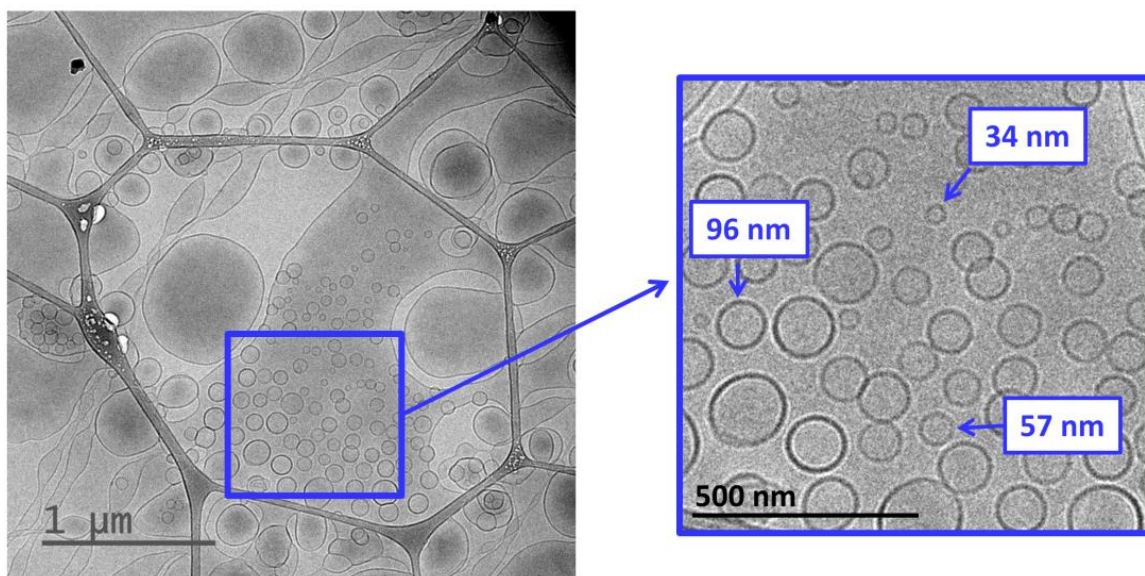


Figure 3: Cryo-TEM image of AOT aggregates at 55CVC (0.5wt%) in brine solution

Then, we investigated a diluted AOT system and detected a small number of surfactant vesicles (Figure 4).

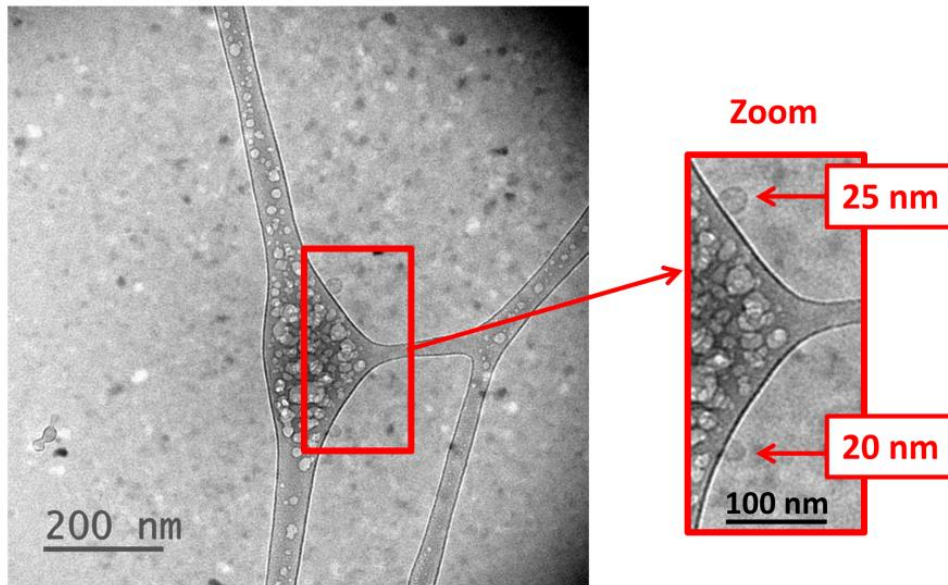


Figure 4: Cryo-TEM image of AOT aggregates at 2.7CVC (0.024wt%) in brine solution

In the following work, we considered vesicles formed in the diluted AOT solution, the latter is referred as *Sol_Ref* (AOT=2.7CVC=0.024wt% in 1.5wt% NaCl).

4.3. DLS

Dynamic light scattering experiments provided the size distribution of AOT vesicles for solution *Sol_Ref*. We consider a diluted system with no inter-particle interactions and no multiple-scattering effects. We assumed that the intensity fluctuations of the scattered light with time is only caused by the random Brownian motion of vesicles in solution (no others contributions such as vesicles fusion ...).

In cryo-TEM images, only vesicles were observed although micelles can be formed for diluted solutions according to the phase diagram. We therefore examined whether there was an equilibrium between micelles and vesicles in solution. For this purpose, auto-correlation functions from a micellar solution (AOT 1wt% with no salt addition) and vesicular solution (AOT 1.3CMC=0.117 g/L in brine) obtained with the VascoKin (Cordouan Technologies) were compared (Figure 5a). Sheu et al.[10] have demonstrated the presence of oblate spheroidal micelles at 1% AOT concentration without salt.

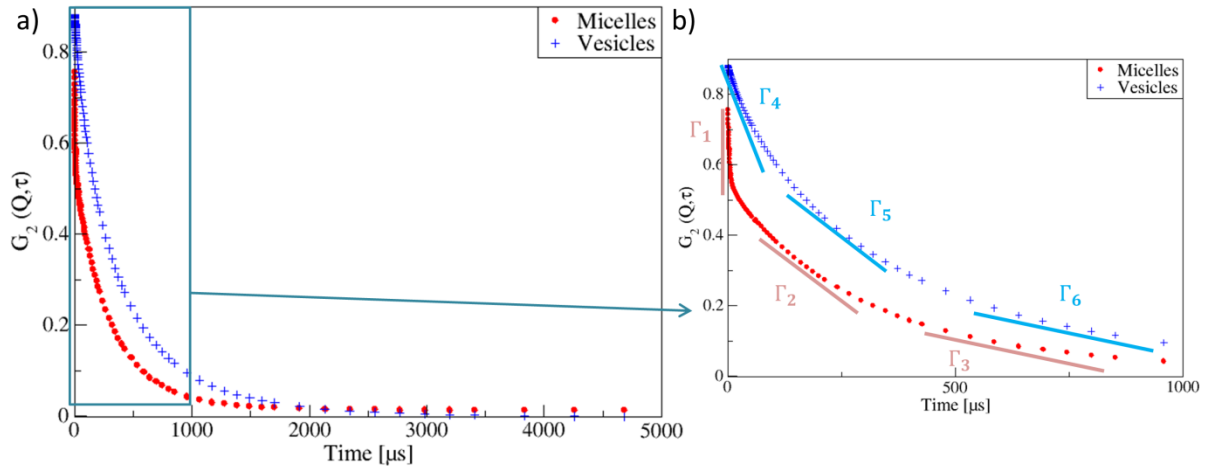


Figure 5: a) Comparison of the autocorrelation functions obtained for a micellar solution (●) and vesicular system (+) with the VascoKin from Cordouan Technologies b) Zoom of the two autocorrelation functions in the section where micellar aggregates can be discriminated

For the micellar solution, we observed in Figure 5b a rather fast decay Γ_1 ($\Gamma_i = D_i Q^2$) corresponding to micellar aggregates followed by two smaller ones Γ_2 and Γ_3 . The existence of the last two slower decays demonstrates that AOT already forms some vesicles in solution with no salt addition. This observation is in agreement with the study performed by Fan et al.[9] on the micellization process of AOT. For the vesicular system, the first decay Γ_4 is slower than Γ_1 , demonstrating the presence of larger aggregates with no micelles in solution : the system is only vesicular.

We used a discrete Pade-Laplace inversion algorithm that is consistent with the polydispersity in vesicle size observed in cryo-TEM picture. The intensity distribution is assumed to be correct if the residuals (difference between experimental data and Pade-Laplace model) is at least five times smaller than the smallest intensity found.

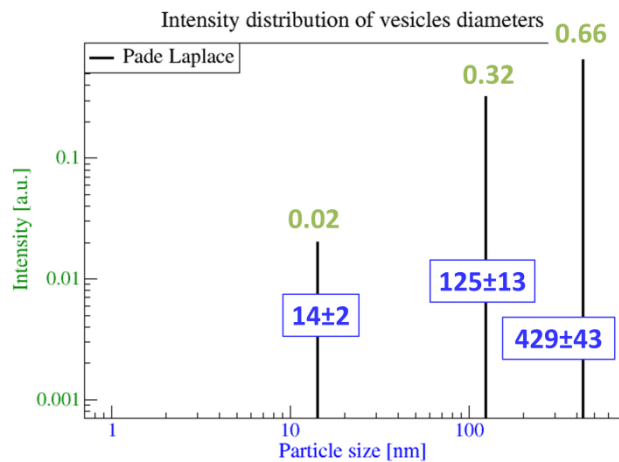


Figure 6: Distribution of the hydrodynamic diameter for *Sol_Ref* and analyzed with Pade-Laplace model

Figure 6 represents the intensity distribution of the scattered light: three populations are observed at 14 nm, 125 and 429 nm in diameters.

Table 4: Normalized number based distribution calculated from RGD approximation for *Sol_Ref* from results presented in Figure 6

Vesicle diameter	Number based distribution
14 nm	0.9976
125 nm	1.80×10^{-3}
429 nm	5.52×10^{-4}

Results presented in Table 4 show the number based distribution calculated from RGD approximation: small vesicles (14 nm) are predominant in solution with a small number of larger vesicles (< 1%). Thus, the surfactant solution is mainly composed of small vesicles of around 14 nm diameter.

4.4. Combination of MALS and SAXS measurements

MALS and SAXS scattering techniques have been combined to cover a large Q range in order to investigate the vesicle structure at different length scales. MALS measurements have been performed with solution *Sol_Ref* and for SAXS, the solution was concentrated to 1wt% of AOT in brine because of the poor contrast between surfactant bilayer and water. In fact, the scattering profile performed with *Sol_Ref* did not provide any different trend compared to the brine scattering profile. We also performed measurements at a smaller concentration (AOT=0.5wt% in brine): the scattering profile is similar to the 1wt% but the scattering curve is noisy. We assumed that the bilayer formed at an AOT concentration of 1wt% is the same as for *Sol_Ref* because SAXS results give the same bilayer structure for 1wt% and 0.5wt% in brine.

For both techniques, scattering intensities have been normalized by the concentration and appropriate contrast term in order to represent data on the same graph (Figure 7a). For MALS, we have plotted $[R(Q) / (K\phi d^2 Na)]$ as a function of Q: d is the surfactant density. For SAXS, we have plotted $[I_x(Q) / (\phi \Delta \rho^2)]$ as a function of Q.

In the chosen model, we assume a symmetric bilayer (outer and inner hydrophilic parts identical). The same form factor can be used for both techniques as explained before and adjustment of experimental data with equation (15) were performed using SASfit software.

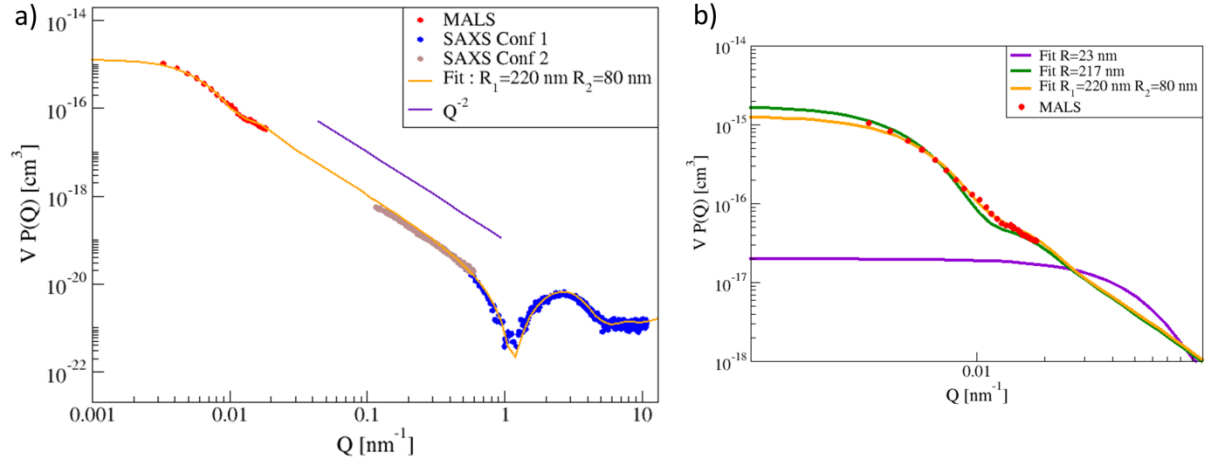


Figure 7: a) Model providing the best fit to experimental data obtained with MALS and SAXS
b) Zoom at low Q-range

Depending on the Q-range, different parameters of the vesicle size and structure can be determined.

4.4.1. Low Q-range

Fitting the data at low Q-range with a single log-normal distribution was not sufficient (green fit in Figure 7b). Thus, we used the sum of two log-normal distributions. The size distribution function is given by :

$$f(R) = \sum_{i=1}^2 \frac{1}{R\sigma_i\sqrt{2\pi}} \exp\left(-\frac{\ln^2(R/\bar{R}_i)}{2\sigma_i^2}\right) \quad (17)$$

with \bar{R} the vesicle mean radius and σ the polydispersity. The following distribution function $f(R, \bar{R}_1 = 220 \text{ nm}, \sigma_1 = 0.26, \bar{R}_2 = 80 \text{ nm}, \sigma_2 = 0.35)$ corresponding to the yellow fit in Figure 7a gives a good adjustment of the small oscillation at $1.3 \times 10^{-2} \text{ nm}^{-1}$ highlighted in the zoom in Figure 7b. \bar{R}_1 and \bar{R}_2 are in good agreement with the largest sizes found in DLS (Figure 6: hydrodynamic radius of 62.5 nm and 214.5 nm). Moreover, we calculated the critical surfactant concentration necessary to be sensitive to the structure factor with the previous vesicles size to be 3wt%. Thus, the assumption that there is no inter-particles interactions is valid.

We obtained the following size distribution (Figure 8):

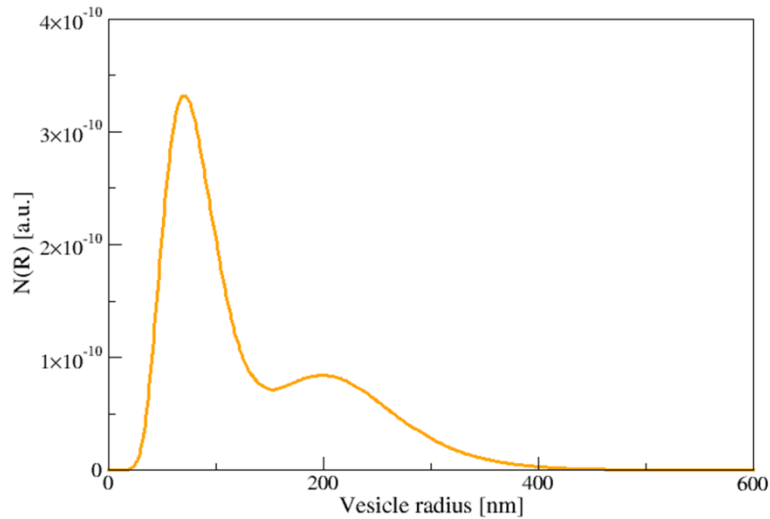


Figure 8: Size distribution obtained with the model presented in Figure 7a

Smaller vesicles than those chosen in the model appear at intermediate Q range as shown by the purple fit in Figure 7b. However, this Q-range was not investigated.

4.4.2. Intermediate Q-range

We can observe a Q^{-2} decrease at intermediate Q range which is indicative of two dimensional aggregates such as unilamellar spherical vesicles[40].

4.4.3. High Q-range

This Q^{-2} decrease is followed by a well-established oscillation around $Q=1 \text{ nm}^{-1}$: this oscillation is characteristic of the bilayer form factor. The analysis of this oscillation provides information on the internal structure and composition of the vesicle bilayer. The maximum intensity in the oscillation appears around $Q=2.5 \text{ nm}^{-1}$ which corresponds to the thickness of the contrasted vesicle part being explored (electron density of the two polar regions and hydrophobic core). The adjustment of experimental data at high Q-range allows the characterization of the surfactant bilayer: the thicknesses of the hydrophilic head group and of the hydrophobic core are 1.2 nm and 0.29 nm respectively with a water volume fraction of 0.95 and 0.03. These results lead to an overall bilayer thickness of 2.7 nm even though the length of the extended AOT molecule is about 1.7 nm[41]. It has been compared to values found in literature, from bilayers in solution or adsorbed on solid surfaces, in Table 5.

Table 5 : AOT bilayer thicknesses reported in the literature

Bilayer	In solution				Adsorbed at solid/liquid interface	
	Reference	Grillo et al.[20]	Grillo et al.[20]	Fontell[3] Nallet et al. [22]	Skouri et al.[4]	Hellsing et al.[42]
AOT bilayer	7.5 g/L AOT / 9.9 g/l NaCl	3.75 g/L AOT / 2.45 g/L NaCl	Lamellar liquid crystalline phase	AOT lamellar phase $L\alpha$	AOT / sapphire	AOT + 0.3 g/L NaCl / sapphire
Thickness [nm]	1.95	1.95	≈ 2	1.95	3.3	2.3

The AOT bilayer thickness in the presence of salt reported in the literature is also smaller than twice the extended AOT length. Regarding the work performed by Hellsing et al. [42], we can clearly predict that the increase in ionic strength tends to decrease the bilayer thickness. In fact, NaCl reduces the electrostatic repulsion between sulfonate hydrophilic head groups enhancing the hydrophobic interaction and allowing closer packing of alkyl chains.

The important hydration of the hydrophilic headgroups may be related to the presence of a large hydrophilic group ($C_4H_7NaO_7S$) composed of highly polar carbonyl groups. Similar results have been found by Wang et al.[43] regarding the adsorption of $Ca(AOT)_2$ on silica : $\phi_{water_head}=0.85$ and $\phi_{water_tail}=0.1$ (with ϕ the water volume fraction).

5. Conclusion

Vesicular AOT aggregates formed in brine (1.5 wt% NaCl) at 20°C in the ultra-low surfactant concentration domain have been investigated by cryo-TEM and the combination of three scattering techniques (SAXS, DLS and MALS). Small vesicles (14 nm diameter) are predominant in solution and there is no vesicle/micelle equilibrium. The small bilayer thickness (2.7 nm) indicates the predominance of hydrophobic interactions between hydrophobic tails in comparison to electrostatic repulsion between sulfonate head groups. This complete characterization was necessary to fully understand the adsorption behavior of AOT on silica that will be investigated by quartz crystal microbalance and neutron reflectivity in further experiments.

Acknowledgements.

The authors thank A. Vacher (Solvay, Aubervilliers) and M. Airiau (Solvay, Aubervilliers) for their contributions in cryo-TEM measurements; D. Frot (IFPEN) for many useful discussions on DLS experiments; A. Suzzoni (IFPEN) and J. M'Hamdi (IFPEN) for their help for synchrotron and MALS measurements respectively. We also acknowledge the Synchrotron SOLEIL (Gif-sur-Yvette, France) for beam time allocation and Cordouan Technologies for results obtained with the VascoKin.

References

- [1] B. Balinov, U. Olsson and O. Soederman, Structural similarities between the L3 and bicontinuous cubic phases in the AOT-brine system, *J. Phys. Chem.* 95 (15) (1991) 5931–5936.
- [2] Ghosh O., C.A. Miller, Liquid-crystalline and microemulsion phase behavior in alcohol-free Aerosol-OT/oil/brine systems, *J. Phys. Chem.* 91 (17) (1987) 4528–4535.
- [3] K. Fontell, The structure of the lamellar liquid crystalline phase in aerosol OT—water system, *Journal of Colloid and Interface Science* 44 (2) (1973) 318–329.
- [4] M. Skouri, J. Marignan, and R. May, X-ray and neutron-scattering study of the lamellar and L3 phases of the system aerosol-OT-water: effect of NaCl and decane, *Colloid and Polymer Science* 269 (9) (1991) 929–937.
- [5] D. Park, J. Rogers, R. W. Toft, AND P. A. Winsor, The Structure of Micellar Solutions of Ionic Amphiphiles: The Lamellar Phase. X-Ray Diffraction Measurements with the Aerosol OT/Water System, *Journal of Colloid and Interface Science* 32 (1) (1970) 81–90.
- [6] E. Franses, T. Hart, Phase behavior and molecular motion of aerosol OT in liquid-crystalline phases with water, *Journal of Colloid and Interface Science* 94 (1) (1983) 1–13.
- [7] J. Rogers, P.A. Winsor, Change in the optic sign of the lamellar phase (G) in the aerosol OT/water system with composition or temperature, *Journal of Colloid and Interface Science* 30 (2) (1969) 247–257.
- [8] M.-F. Ficheux A.-M. Bellocq, F. Nallet, Effect of two water-soluble polymers on the stability of the AOT-H₂O-lamellar phase, *Colloids and Surfaces A: Physicochemical and Engineering Aspects* 123-124 (1997) 253–263.
- [9] Y. Fan, Y. Li, G. Yuan, Y. Wang, J. Wang, C.C. Han, H. Yan, Z. Li, R.K. Thomas, Comparative studies on the micellization of sodium bis(4-phenylbutyl) sulfosuccinate and sodium bis(2-ethylhexyl) sulfosuccinate and their interaction with hydrophobically modified poly(acrylamide), *Langmuir the ACS journal of surfaces and colloids* 21 (9) (2005) 3814–3820.
- [10] E. Y. Sheu, S. H. Chen and J. S. Huang, Structure and growth of bis(2-ethylhexyl) sulfosuccinate micelles in aqueous solutions, *J. Phys. Chem.* 91 (12) (1987) 3306–3310.
- [11] I. M. Umlong and K. Ismail, Micellization of AOT in aqueous sodium chloride, sodium acetate, sodium propionate, and sodium butyrate media: a case of two different concentration regions of counterion binding, *Journal of Colloid and Interface Science* 291 (2) (2005) 529–536.
- [12] J. Dey, J. Bhattacharjee, P.A. Hassan, V.K. Aswal, S. Das, K. Ismail, Micellar shape driven counterion binding. Small-angle neutron scattering study of AOT micelle, *Langmuir the ACS journal of surfaces and colloids* 26 (20) (2010) 15802–15806.
- [13] I. Grillo, E.I. Kats, A.R. Muratov, Formation and Growth of Anionic Vesicles Followed by Small-Angle Neutron Scattering, *Langmuir* 19 (11) (2003) 4573–4581.
- [14] J. Bergenholtz, N.J. Wagner, Formation of AOT/Brine Multilamellar Vesicles, *Langmuir* 12 (13) (1996) 3122–3126.
- [15] Annalisa Caria and Ali Khan, Phase Behavior of Catanionic Surfactant Mixtures: Sodium Bis(2-ethylhexyl)sulfosuccinate–Didodecyldimethylammonium bromide–Water System, *Langmuir* 12 (1996) 6282–6290.
- [16] N. Shahidzadeh, D. Bonn and J. Meunier, A new mechanism of spontaneous emulsification: Relation to surfactant properties, *EPL* 40 (4) (1997) 459–464.
- [17] O. Regev and A. Khan, Vesicle. lamellar transition events in DDAB-water solution, *Progr Colloid Polym Sc* 97 (1994) 298–301.

- [18] Y. Jiang, F. Li, Y. Luan, W. Cao, X. Ji, L. Zhao, L. Zhang, Z. Li, Formation of drug/surfactant catanionic vesicles and their application in sustained drug release, *International journal of pharmaceutics* 436 (1-2) (2012) 806–814.
- [19] J. Liu, Y. Jiang, Y. Cui, C. Xu, X. Ji, Y. Luan, Cytarabine-AOT catanionic vesicle-loaded biodegradable thermosensitive hydrogel as an efficient cytarabine delivery system, *International journal of pharmaceutics* 473 (1-2) (2014) 560–571.
- [20] I. Grillo, P. Levitz, T. Zemb, Insertion of Small Anionic Particles in Negatively Charged Lamellar Phases, *Langmuir* 16 (11) (2000) 4830–4839.
- [21] C. Boissière, J.B. Brubach, A. Mermet, G. de Marzi, C. Bourgaux, E. Prouzet, P. Roy, Water Confined in Lamellar Structures of AOT Surfactants: An Infrared Investigation, *J. Phys. Chem. B* 106 (5) (2002) 1032–1035.
- [22] F. Nallet, R. Laversanne and D. Roux, Modelling X-ray or neutron scattering spectra of lyotropic lamellar phases interplay between form and structure factors, *J. Phys. II France* 3 (1993) 487–502.
- [23] S.T. Hyde, Microstructure of bicontinuous surfactant aggregates, *J. Phys. Chem.* 93 (4) (1989) 1458–1464.
- [24] Oren Regev/Changjiang Kang/Ali Khan, Cryo-TEM and NMR Studies of Solution Microstructures of Double-Tailed Surfactant Systems: Didodecyldimethylammonium Hydroxide, Acetate, and Sulfate.
- [25] V. Bergeron, Microtubes Created in Thin Liquid Films during Bilayer Adhesion and Fusion, *Langmuir* 12 (24) (1996) 5751–5755.
- [26] J.I. Briz, M.M. Velázquez, Effect of water-soluble polymers on the morphology of aerosol OT vesicles, *Journal of Colloid and Interface Science* 247 (2) (2002) 437–446.
- [27] P.J. Wyatt, Light scattering and the absolute characterization of macromolecules, *Analytica Chimica Acta* 272 (1) (1993) 1–40.
- [28] O. Glatter and O. Kratky, *Small Angle X-Ray Scattering*, Academic Press (1982).
- [29] Bruce J. Berne and Robert Pecora, *Dynamic Light scattering: with applications to chemistry, biology, and physics*, A Wiley interscience publication, 1976.
- [30] G. White, J. Pencer, B.G. Nickel, J.M. Wood, F.R. Hallett, Optical changes in unilamellar vesicles experiencing osmotic stress, *Biophysical journal* 71 (5) (1996) 2701–2715.
- [31] F.R. Hallett, J. Watton, P. Krygsman, Vesicle sizing, *Biophysical journal* 59 (2) (1991) 357–362.
- [32] J. Pencer, F.R. Hallett, Effects of Vesicle Size and Shape on Static and Dynamic Light Scattering Measurements, *Langmuir* 19 (18) (2003) 7488–7497.
- [33] J.H. van Zanten, H.G. Monbouquette, Characterization of vesicles by classical light scattering, *Journal of Colloid and Interface Science* 146 (2) (1991) 330–336.
- [34] S. Kölchens, V. Ramaswami, J. Birgenheier, L. Nett, D.F. O'Brien, Quasi-elastic light scattering determination of the size distribution of extruded vesicles, *Chemistry and Physics of Lipids* 65 (1) (1993) 1–10.
- [35] B. Lange, S.R. Aragón, Mie scattering from thin anisotropic spherical shells, *The Journal of chemical physics* 92 (8) (1990) 4643–4650.
- [36] S. R. Aragon and R. Pecora, Theory of dynamic light scattering from large anisotropic particles, *The Journal of chemical physics* 66 (6) (1977) 2506–2516.
- [37] G. Fragneto, Z.X. Li, R.K. Thomas, A.R. Rennie, J. Penfold, A Neutron Reflectivity Study of the Adsorption of Aerosol-OT on Self-Assembled Monolayers on Silicon, *Journal of Colloid and Interface Science* 178 (1996) 531–537.
- [38] I. Grillo, J. Penfold, Self-assembly of mixed anionic and nonionic surfactants in aqueous solution, *Langmuir the ACS journal of surfaces and colloids* 27 (12) (2011) 7453–7463.

- [39] J. Kuntsche, J.C. Horst, H. Bunjes, Cryogenic transmission electron microscopy (cryo-TEM) for studying the morphology of colloidal drug delivery systems, *International journal of pharmaceutics* 417 (1-2) (2011) 120–137.
- [40] P.W. Schmidt, Interpretation of small-angle scattering curves proportional to a negative power of the scattering vector, *J Appl Crystallogr* 15 (5) (1982) 567–569.
- [41] S. P. Moulik and K. Mukherjee, Review article: On the versatile surfactant aerosol-ot (AOT): its physicochemical and surface chemical behaviours and uses, *Proc. Indian natn. Sci. Acad.* 62 (3) (1996) 215–232.
- [42] M.S. Helling, A.R. Rennie, A.V. Hughes, Effect of concentration and addition of ions on the adsorption of aerosol-OT to sapphire, *Langmuir the ACS journal of surfaces and colloids* 26 (18) (2010) 14567–14573.
- [43] X. Wang, S. Y. Lee, K. Miller, R. Welbourn, I. Stocker, S. Clarke, M. Casford, P. Gutfreund and M. W. A. Skoda, Cation bridging studied by specular neutron reflection, *Langmuir the ACS journal of surfaces and colloids* 29 (18) (2013) 5520–5527.